Network and geometric characterization of three-dimensional fluid transport between two layers

Rebeca de la Fuente [ORCID],[1] Gábor Drótos [ORCID],[1,2] Emilio Hernández-García [ORCID],[1] and Cristóbal López [ORCID][1]

[1]*IFISC (CSIC-UIB), Instituto de Física Interdisciplinar y Sistemas Complejos, E-07122 Palma de Mallorca, Spain*
[2]*MTA-ELTE Theoretical Physics Research Group, H-1117 Budapest, Hungary*

We consider transport in a fluid flow of arbitrary complexity but with a dominant flow direction. One of the situations in which this occurs is when describing by an effective flow the dynamics of sufficiently small particles immersed in a turbulent fluid and vertically sinking because of their weight. We develop a formalism characterizing the dynamics of particles released from one layer of fluid and arriving in a second one after traveling along the dominant direction. The main ingredient in our study is the definition of a two-layer map that describes the Lagrangian transport between both layers. We combine geometric approaches and probabilistic network descriptions to analyze the two-layer map. From the geometric point of view, we express the properties of lines, surfaces, and densities transported by the flow in terms of singular values related to Lyapunov exponents, and define a specific quantifier, the finite depth Lyapunov exponent. Within the network approach, degrees and an entropy are considered to characterize transport. We also provide relationships between both methodologies. The formalism is illustrated with numerical results for a modification of the ABC flow, a model commonly studied to characterize three-dimensional chaotic advection.

I. INTRODUCTION

The study of transport phenomena is at the core of fluid mechanics. The Lagrangian approach to fluid transport has received powerful insights from its relationship to chaos and dynamical systems [1–3], and more recently from set-oriented methodologies which can be recast into the language of graph or network theory [4–7].

In most of the previous applications of these developments to geophysical contexts, consideration has been restricted to horizontal transport, as this is the dominant mode of motion at large scales in oceans and in the atmosphere. Some works, however, have addressed the full three-dimensional dynamics [8–10]. Less attention has been given to the application or adaptation of the approaches mentioned above to the peculiarities of transport in the vertical direction, which is singled out by the gravitational force.

As the main motivation for the present work, many relevant biogeochemical phenomena involve the vertical transport of particles in the ocean. Two paradigmatic examples are the sinking of biogenic particles [11,12], like phytoplankton cells and marine snow, which play a fundamental role in the biological carbon pump [13,14], and the sedimentation dynamics of microplastics, which are becoming a key environmental problem [15–17]. Despite the numerous studies with different experimental and theoretical methodologies many questions remain open, in particular those concerning the final fate of the particles from a known release surface area (i.e., the connection paths between surface and deep ocean), the amount and time they are suspended in the water column, and the spatial distribution over both the water column and the seafloor. Beyond the ocean context, vertical transport is also relevant in many other situations such as engineering processes [18] or rain precipitation [19].

The objective of this paper is to extend and adapt the powerful Lagrangian methodologies previously commented on to dynamics for which there is a strong anisotropy in the particle motion, leading to a clear transport direction. This is the case when considering sinking particles in fluid flows. We will concentrate on characterizing transport between two layers: in the case of particles sedimenting under gravity, particles released from an upper layer are driven by the flow and reach and accumulate in a lower layer. We expect our formalism would be useful also under transport anisotropies produced by forces other than gravity. The main object we will define is a two-layer map that connects the initial conditions of particles released from one of the layers to their final positions in the other one, after being transported by the flow. We extract information from this map with the two complementary approaches mentioned above: on the one hand we use dynamical systems tools to describe the geometry of the evolution of sheets of particles released from the initial layer. In this way we formalize previous results obtained in this context [20–22] and extend them by the introduction of a specific quantifier related to Lyapunov exponents: the finite depth Lyapunov exponent. On the other hand, connectivity properties between the layers are studied with network theory or probabilistic techniques. Relationships between both approaches are obtained, and the whole formalism is illustrated with a modification of the ABC flow. This flow model is frequently used as a simple example of three-dimensional chaotic advection, to which we add an additional constant velocity in the vertical direction to model sinking.

The outline of the paper is as follows. In Sec. II we introduce the basic Lagrangian description for transport of particles between two layers. In Sec. III we study the geometry and dynamics of a falling layer of particles, introducing the finite depth Lyapunov exponent. In Sec. IV we introduce the network methods to characterize connectivity, and in Sec. V we show the connection between the previous two descriptions. In Sec. VI we present the numerical results obtained for the modified ABC flow model. Section VII presents our conclusions. An Appendix contains additional technical details.

II. CHARACTERIZATION OF TRANSPORT BETWEEN TWO LAYERS

Given a fluid flow characterized by a velocity field $\mathbf{v}(\mathbf{r}, t)$, the Lagrangian description of transport considers the equations of motion for the position of fluid elements, which evolve according to.

$$\frac{d\mathbf{r}(t)}{dt} = \mathbf{v}(\mathbf{r}(t), t). \tag{1}$$

This equation defines the flow map $\phi_{t_0}^{\tau}(\mathbf{r}_0)$, such that integrating Eq. (1) for a given initial condition $\mathbf{r}_0$ at t_0 gives the final position of the particle at time $t_0 + \tau$:

$$\phi_{t_0}^{\tau}(\mathbf{r}_0) = \mathbf{r}(t_0 + \tau). \tag{2}$$

In the rest of the paper, we will restrict to the situation in which $\mathbf{v}(\mathbf{r}(t), t)$ is a three-dimensional velocity field, and trajectories $\mathbf{r}(t)$ move in regions of $\mathbb{R}^3$.

Description (1) is pertinent not only for the motion of fluid elements. Particles of other substances immersed in a fluid also satisfy a first-order equation like (1), provided they are sufficiently small for their inertia to be neglected. For example, in a variety of realistic situations in the ocean, the equation of motion for the position of many types of particles of biological origin or of microplastics is ruled by Eq. (1), in which the velocity field is replaced by the actual velocity of the fluid flow with an added constant vertical component related to the sinking of the particle under gravity because of its weight [11,12,17]. In this paper we will refer to the motion of "particles" without specifying if they are particles of fluid or particles submerged in a fluid. In both cases the dynamics is provided by an equation of the type (1), and thus Eq. (2) applies.

An object that plays an important role in the analysis of the map in (2) is its Jacobian matrix (a 3×3 matrix), defined by

$$\mathbf{J} = \nabla \phi_{t_0}^{\tau}(\mathbf{r}_0). \tag{3}$$

Given an infinitesimal separation between two initial conditions $d\mathbf{r}_0$, $\mathbf{J}$ gives the evolution in time of this separation: $d\mathbf{r}(t_0 + \tau) = \mathbf{J} \cdot d\mathbf{r}_0$. The singular values $\{S_{\alpha}\}_{\alpha=1,2,3}$ of $\mathbf{J}$ (i.e., the square roots of the eigenvalues of the Cauchy-Green tensor $C = \mathbf{J}^T \mathbf{J}$) give the stretching factors experienced by infinitesimal material line elements oriented along the eigendirections and initialized around $\mathbf{r}_0$ while integrated from t_0 to $t_0 + \tau$. The standard finite-time Lyapunov exponents (FTLEs, $\{\lambda_{\alpha}\}_{\alpha=1,2,3}$) are obtained from these singular values as $\lambda_{\alpha} = |\tau|^{-1} \ln S_{\alpha}$ [3].

In this paper we are interested in anisotropic situations in which a direction of flow is distinguished from the others.

Specifically, instead of the fully three-dimensional motion described by $\phi_{t_0}^{\tau}$, we are interested in the dynamics of particles traveling between a pair of two-dimensional layers. The main example is the case of particles released from an upper horizontal layer, falling by gravity across a moving flow, and being collected on a second, lower horizontal layer. Other sources of anisotropy can play the role of gravity, but in this paper we use the terminology appropriate to the sedimentation by gravity example, so that both layers will be considered to be horizontal. The first layer will be called the *upper* or *release* layer, whereas the second one will be called the *lower* or the *collecting* layer. We distinguish the *vertical* coordinate z from the *horizontal* ones that form the horizontal vector $\mathbf{x}$, so that $\mathbf{r} = (x, y, x) \equiv (\mathbf{x}, z)$. Particles are initially released (at t_0) from the horizontal layer $\mathcal{M}$ characterized by "height" z_0: $\mathcal{M} \equiv \{\mathbf{r} = (\mathbf{x}_0, z_0), z_0 \text{ fixed}\}$, and we want to track the horizontal position $\mathbf{x}$ at which the particle started at $\mathbf{r}_0$ first reaches the second horizontal layer characterized by "depth" z. As we stop the dynamics after this first arrival, we can say that particles "accumulate" at the second layer. This procedure defines a flow map which we call the *two-layer map*: $\mathbf{x} = \phi_{z_0}^{z}(\mathbf{x}_0)$. We do not explicitly specify the initial time t_0, but for time-dependent velocity fields there will be a dependence on it.

Given a region $D \in \mathcal{M}$ of the upper layer, we call its image $\phi_{z_0}^{z}(D)$ onto the lower one its *footprint*. It is the region of the collecting layer where particles from D will become accumulated.

Particles released at the same time do not necessarily arrive at the same time at the final layer. Let $\omega(\mathbf{x}_0)$ be the time that a particle started at t_0 from $(\mathbf{x}_0, z_0)$ takes to reach the second layer at z for the first time. Thus the time of arrival is $t_z = t_0 + \omega$. Although not explicitly written, ω and t_z depend on t_0, z_0 and z, in addition to $\mathbf{x}_0$. In terms of ω, the relationship between the coordinates of the two flow maps introduced so far is

$$\phi_{z_0}^{z}(\mathbf{x}_0) = \mathbf{x}[t_0 + \omega(\mathbf{x}_0)] = \phi_{t_0}^{\omega(\mathbf{x}_0)}[\mathbf{r} = (\mathbf{x}_0, z_0)]|_h,$$
$$z = \phi_{t_0}^{\omega(\mathbf{x}_0)}[\mathbf{r} = (\mathbf{x}_0, z_0)]|_z, \tag{4}$$

where the subindices h and z indicate that the horizontal and vertical coordinates of $\phi_{t_0}^{\omega}$, respectively, should be taken.

In general $\phi_{z_0}^{z}$ can be computed by solving Eq. (1) from initial conditions on $\mathcal{M}$, and checking when the trajectory crosses the second layer at z, as Eq. (4) indicates. In this paper we will use this last method.

The Jacobian associated with the two-layer map is

$$\bar{\mathbf{J}}_{\mathcal{M}} = \nabla \phi_{z_0}^{z}(\mathbf{x}_0). \tag{5}$$

Note that the gradient acts on the two-dimensional initial position $\mathbf{x}_0$, so that $\bar{\mathbf{J}}_{\mathcal{M}}$ is a 2×2 matrix. The subindex $\mathcal{M}$ is a reminder of the fact that $\bar{\mathbf{J}}_{\mathcal{M}}$ is defined on each point $\mathbf{x}_0$ of the upper layer $\mathcal{M}$.

The singular values of this twodimensional Jacobian matrix are the square roots of the eigenvalues of the associated 2×2 Cauchy-Green tensor:

$$\bar{C}_{\mathcal{M}} = \left[\nabla \phi_{z_0}^{z}(\mathbf{x}_0)\right]^T \cdot \nabla \phi_{z_0}^{z}(\mathbf{x}_0), \tag{6}$$

which will be used later.

We next develop the two complementary approaches we propose to study transport between two layers: the geometric and the network approaches.

III. GEOMETRIC CHARACTERIZATION OF A FALLING LAYER

First, we introduce a geometric characterization of the deformation of the falling layer of released particles with tools from dynamical systems. This approach can be called either *geometric* or *dynamical*.

In the same way that the three-dimensional Jacobian matrix $\mathbf{J}$ maps infinitesimal vector particle separations from time t_0 to time t ($d\mathbf{r}(t) = \mathbf{J} \cdot d\mathbf{r}_0$), $\bar{\mathbf{J}}_{\mathcal{M}}$ takes initial infinitesimal separations $d\mathbf{x}_0$ on the horizontal release layer and gives its footprint $d\mathbf{x}_z$ on the collecting layer: $d\mathbf{x}_z = \bar{\mathbf{J}}_{\mathcal{M}} \cdot d\mathbf{x}_0$. The singular values $\bar{\Lambda}_1$ and $\bar{\Lambda}_2$ of $\bar{\mathbf{J}}_{\mathcal{M}}$ give the stretching factors experienced by the footprint of line elements initially oriented along the eigendirections of $\bar{C}_{\mathcal{M}}$. In analogy with the definition of FTLEs, we can define *finite-depth Lyapunov exponents* [FDLEs, $\bar{\lambda}_\alpha(\mathbf{x}_0)$] as the logarithmic rate of stretching along the eigendirections:

$$\bar{\lambda}_\alpha(\mathbf{x}_0) = \frac{1}{|z - z_0|} \log \bar{\Lambda}_\alpha, \alpha = 1, 2. \tag{7}$$

$\bar{\lambda}_\alpha$ is naturally expressed as a function of $\mathbf{x}_0$. But in fact it is a property of the trajectory joining $\mathbf{x}_0$ and $\mathbf{x} = \phi_{z_0}^z(\mathbf{x}_0)$, so that it (and $\bar{\Lambda}_\alpha$) can be thought of and displayed as a function of the coordinates on the collecting layer, $\mathbf{x}$. Although not explicitly indicated, $\bar{\lambda}_\alpha$ (and $\bar{\Lambda}_\alpha$) is a function of t_0, z_0, and z. Values $\bar{\lambda}_\alpha > 0$ ($\bar{\Lambda}_\alpha > 1$) indicate growth of lengths initially oriented along the corresponding eigendirection, whereas $\bar{\lambda}_\alpha < 0$ ($\bar{\Lambda}_\alpha < 1$) indicate length contraction. If $\bar{\lambda}_1 > \bar{\lambda}_2$, for sufficiently large differences of depth $|z - z_0|$, we would have $|d\mathbf{x}_z| \approx e^{|z-z_0|\bar{\lambda}_1} |d\mathbf{x}_0^{(1)}|$, where $d\mathbf{x}_0^{(1)}$ is the projection of the initial particle separation $d\mathbf{x}_0$ onto the singular vector of singular value $\bar{\Lambda}_1$.

At difference with the FTLE, the FDLE has dimensions of inverse of length, not of time. But this is not the most important difference between the two quantities [in fact, an alternative definition could be to replace $|z - z_0|$ by ω in (7)]. The main difference is that the FTLE quantifies the stretching of initial vectors as they are transported by the flow in three-dimensional space, whereas the FDLE also includes the projection effect experienced by these vectors when arriving at the collecting layer: the footprint of such a vector is the projection onto the horizontal layer of that vector arriving there, taken along its direction of motion. Further details of this projection process are given in the Appendix and are illustrated in Fig. 1. Note also that the FDLE is not a form of a finite-size Lyapunov exponent [23–25], since for this last quantity initial separations are integrated until reaching a specified separation value, whereas in the FDLE integration proceeds until reaching a particular depth level z.

Next, we consider the effect of the flow on surface elements initially located in the release layer. This was already studied in [12,20–22] in the context of sedimenting particles in fluid flows.

Let us consider an infinitesimal material surface of area dA_0 started at the release layer at z_0, which at any time is

$$dA_0 = |\boldsymbol{\tau}_x(t_0) \times \boldsymbol{\tau}_y(t_0)| dx_0 dy_0 = dx_0 dy_0$$

$$dA_t = |\boldsymbol{\tau}_x(t) \times \boldsymbol{\tau}_y(t)| dA_0$$

$$\bar{\boldsymbol{\tau}} = \hat{\boldsymbol{z}} \times \left(\boldsymbol{\tau} \times \frac{\boldsymbol{v}}{v_z} \right)$$

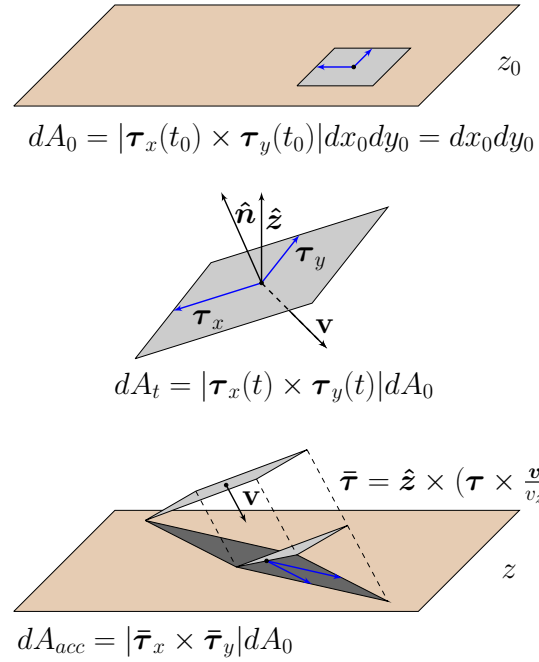$$dA_{acc} = |\bar{\boldsymbol{\tau}}_x \times \bar{\boldsymbol{\tau}}_y| dA_0$$

FIG. 1. Illustration of the dynamics of a rectangular surface element, lying on the upper layer at the release time t_0, and with area dA_0, until leaving a footprint of area dA_{acc} on the lower layer when arriving there. See the discussion and the Appendix for details.

transformed into a surface of area dA_t, and which finally reaches the collecting layer at z leaving a footprint area dA_{acc} (see Fig. 1). If we take the initial surface element to be a rectangle of sides given by the vectors $\hat{\mathbf{x}} dx_0$ and $\hat{\mathbf{y}} dy_0$ ($\hat{\mathbf{x}}$ and $\hat{\mathbf{y}}$ are unit vectors in the x and y directions; the area of the rectangle is $dA_0 = dx_0 dy_0$), and noting that the cross product of vectors gives the area of the parallelogram subtended by them, we obtain

$$dA_{acc} = |\bar{\boldsymbol{\tau}}_x \times \bar{\boldsymbol{\tau}}_y| dA_0, \tag{8}$$

where $\bar{\boldsymbol{\tau}}_x = \frac{\partial \phi_{z_0}^z(\mathbf{x}_0)}{\partial x_0}$ and $\bar{\boldsymbol{\tau}}_y = \frac{\partial \phi_{z_0}^z(\mathbf{x}_0)}{\partial y_0}$ are two-dimensional vectors on the final layer such that $\bar{\boldsymbol{\tau}}_x dx_0$ and $\bar{\boldsymbol{\tau}}_y dy_0$ give the footprint of the initial vectors $\hat{\mathbf{x}} dx_0$ and $\hat{\mathbf{y}} dy_0$.

Simple algebra relates the cross product in (8) to the matrix $\bar{C}_{\mathcal{M}}$ and the singular values $\bar{\Lambda}_\alpha$:

$$|\bar{\boldsymbol{\tau}}_x \times \bar{\boldsymbol{\tau}}_y| = \sqrt{\det \bar{C}_{\mathcal{M}}} = \bar{\Lambda}_1 \bar{\Lambda}_2 \equiv F^{-1}, \tag{9}$$

where we have defined the quantity F, which we call the *density factor*. It is a function of the trajectory that starts at $\mathbf{x}_0$ and arrives at $\mathbf{x} = \phi_{z_0}^z(\mathbf{x}_0)$, so that, with some abuse of language, it can be considered as a function either of the initial or of the final location: $F = F(\mathbf{x}_0)$ or $F = F(\mathbf{x})$. The name "density factor" comes from the consideration of the ratio between the density of particles in a release surface element, $\sigma(\mathbf{x}_0)$, and in its image in the collecting layer $\sigma[\mathbf{x} = \phi_{z_0}^z(\mathbf{x}_0)]$. In the situation in which both surface elements contain the same particles, this ratio is the inverse of the ratio of areas and thus equal to F:

$$\frac{\sigma(\mathbf{x})}{\sigma(\mathbf{x}_0)} = \frac{dA_0}{dA_{acc}} = F. \tag{10}$$

The surface elements dA_0 and dA_{acc} will contain the same particles if a single surface element from the release layer reaches dA_{acc}. For time-dependent velocity fields, folding of the falling layer can occur, and in this case the complete density ratio should be computed as the sum of all contributions of the type (10) from the initial release areas dA_0 that reach the same dA_{acc} at different times [20–22].

A convenient way to write $F = dA_0/dA_{acc}$ is to split it into two contributions [20–22] (see Fig. 1): the evolution of the surface element under the time map $\phi_{t_0}^{\omega}$ until when its area gets stretched to dA_{t_z} (recall that $t_z = t_0 + \omega$ is the time at which the infinitesimal surface touches the z layer), and the projection of this surface element onto the horizontal collecting layer along the direction of motion. The combination of both processes leaves a footprint of area dA_{acc} on the bottom layer, completing the action of $\phi_{z_0}^z$:

$$F = \frac{dA_0}{dA_{t_z}} \frac{dA_{t_z}}{dA_{acc}} = SP. \tag{11}$$

The stretching and projection factors, S and P, can be calculated as [20–22]

$$S = \frac{dA_0}{dA_{t_z}} = |\boldsymbol{\tau}_x(t_z) \times \boldsymbol{\tau}_y(t_z)|^{-1}, \tag{12}$$

$$P = \frac{dA_{t_z}}{dA_{acc}} = \left| \frac{v_z}{\hat{\mathbf{n}} \cdot \mathbf{v}} \right|, \tag{13}$$

where $\hat{\mathbf{n}}(t)$ is a unit vector normal to the falling surface element at time t, and the vectors $\boldsymbol{\tau}_x(t)$ and $\boldsymbol{\tau}_y(t)$ are tangent to the sinking surface dA_t at time t, given by $\boldsymbol{\tau}_x = \frac{\partial \phi_{t_0}^{\tau}(\mathbf{r}_0)}{\partial x_0}$ and $\boldsymbol{\tau}_y = \frac{\partial \phi_{t_0}^{\tau}(\mathbf{r}_0)}{\partial y_0}$. The expression for S is obtained simply by recognizing that $\boldsymbol{\tau}_x(t) \, dx_0$ and $\boldsymbol{\tau}_y(t) \, dy_0$ are the images under time evolution of the vectors $\hat{\mathbf{x}} \, dx_0$ and $\hat{\mathbf{y}} \, dy_0$, respectively, that make the initial surface, and thus the area at any time t is $dA_t = |\boldsymbol{\tau}_x(t) \times \boldsymbol{\tau}_y(t)| \, dx_0 \, dy_0$. A derivation of the expression for P is given in the Appendix, where further details on the projection process are given. As with λ_α, expression (12) is a property of the trajectory joining $\mathbf{x}_0$ and the corresponding $\mathbf{x}$ in the collecting layer, so that S can be considered as a function of any of these two locations. Equation (13) involves velocities and the normal to the surface element at the collecting layer, so that it is more natural to consider $P = P(\mathbf{x})$, although for invertible $\phi_{z_0}^z$ the values of P can also be mapped back to the release layer and displayed there.

The density factor F can also be expressed in terms of singular values of a different Jacobian matrix. We begin with expressing the stretching factor S. First, note that the Jacobian matrix in (3) has as columns the two vectors $\boldsymbol{\tau}_x(t)$, $\boldsymbol{\tau}_y(t)$ and the additional one $\boldsymbol{\tau}_z(t) = \frac{\partial \phi_{t_0}^{\tau}(\mathbf{r}_0)}{\partial z_0}$. Let $\boldsymbol{J}_{\mathcal{M}}$ be the 3×2 matrix having as columns just the three-dimensional vectors $\boldsymbol{\tau}_x(t)$, $\boldsymbol{\tau}_y(t)$. The subindex $\mathcal{M}$ indicates that it involves derivatives only along the horizontal release layer $\mathcal{M}$. The singular values of $\boldsymbol{J}_{\mathcal{M}}$, Λ_1, and Λ_2, are the square roots of the eigenvalues of the 2×2 matrix $C_{\mathcal{M}} = \boldsymbol{J}_{\mathcal{M}}^T \boldsymbol{J}_{\mathcal{M}}$. Simple algebra demonstrates that

$$S^{-1} = |\boldsymbol{\tau}_x(t) \times \boldsymbol{\tau}_y(t)| = \sqrt{\det C_{\mathcal{M}}} = \Lambda_1 \Lambda_2. \tag{14}$$

We stress that the quantities Λ_α are in general different from the singular values S_α of the 3×3 matrix $\boldsymbol{J}$ in Eq. (3), giving
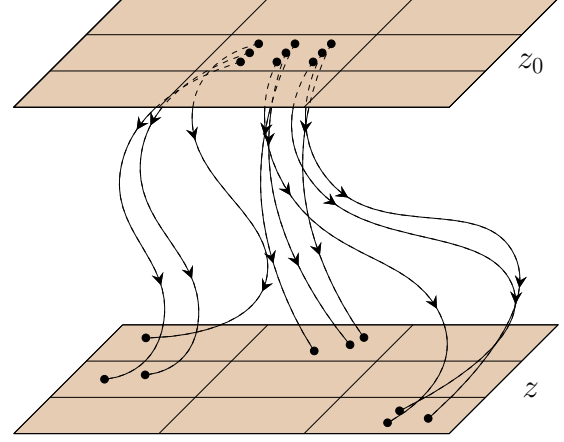

FIG. 2. Sketch of the bipartite network construction. Particles travel from the upper layer to the bottom one. Nodes are the boxes A_i, $i = 1, \ldots, M_0$ on which the upper layer is partitioned, and B_j, $j = 1, \ldots, M_z$, partitioning the lower one. Two nodes are linked if some trajectory joins them.

the Lyapunov exponents as $\lambda_\alpha = |\omega|^{-1} \log S_\alpha$. Λ_α characterizes stretching only of infinitesimal initial vectors lying on the horizontal initial layer. But, in the limit of large t_z or $|z - z_0|$, vectors of arbitrary initial orientation are expected to approach the directions that stretch faster under the action of $\boldsymbol{J}$, so that we expect that in this limit Λ_α will approach S_α, for $\alpha = 1, 2$. More in general, since $\boldsymbol{J}_{\mathcal{M}}$ is the matrix $\boldsymbol{J}$ with a column deleted, inequalities for singular values of submatrices [26] lead to $S_{\alpha+1} \leqslant \Lambda_\alpha \leqslant S_\alpha$, with $\alpha = 1, 2$.

Comparison of Eqs. (9), (11), and (14) gives the following relationship between the descriptions based on the singular values of $\bar{J}_{\mathcal{M}}$ and $J_{\mathcal{M}}$:

$$\bar{\Lambda}_1 \bar{\Lambda}_2 = P^{-1} \Lambda_1 \Lambda_2 = F^{-1}, \tag{15}$$

which also shows the two different ways to compute the density factor F.

IV. THE NETWORK APPROACH

We now describe a characterization of fluid transport between layers by tools from network or graph theory. This type of approach can also be called *probabilistic* or *set-oriented*. Our goal is to generalize studies such as [5,27] by considering a bipartite network, which is the natural framework to study two-layer transport. For this we construct the discrete version of the Perron–Frobenius operator describing the transport matrix between the two layers.

A. Coarse graining of the flow and transport matrix

The upper layer is partitioned with a set of boxes $\{A_i\}_{i=1,\ldots,M_0}$, and the lower layer with boxes $\{B_j\}_{j=1,\ldots,M_z}$ (see Fig. 2). Each of these boxes is interpreted as a node in a bipartite network. Links between the upper and the lower layer are established by the action of the two-layer map. These links are directed and weighted, with weights between A_i in the upper layer and B_j in the lower one given by the proportion of area of A_i that is mapped onto B_j, which defines a transport

matrix:

$$\mathbf{P}(z_0, z)_{ij} = \frac{\mu\left[A_i \bigcap \left(\phi_{z_0}^z\right)^{-1}(B_j)\right]}{\mu(A_i)}. \qquad (16)$$

$\mu(S)$ is the measure of set S (a part of the release layer) here taken to be its area. The map $(\phi_{z_0}^z)^{-1}$ is the inverse of $\phi_{z_0}^z$, i.e., it takes points from the lower layer that at some moment were reached by the released particles and maps them back into the position they had at t_0 in the upper layer. Note that for time-dependent velocity fields this inverse map can be multivalued, as several initial conditions $\mathbf{x}_0$ can reach the same point in the lower layer, provided they do so at different times. In this case, all preimages of box B_j should be considered in Eq. (16). From a practical point of view, one computes the matrix elements $\mathbf{P}(z_0, z)_{ij}$ by releasing a large number N_i of trajectories from box A_i at t_0, and counts how many of them, N_{ij}, reach the collecting layer for the first time at box B_j. The ratio N_{ij}/N_i estimates the value of $\mathbf{P}(z_0, z)_{ij}$ for N_i large enough.

We note that the transport matrix $\mathbf{P}(z_0, z)$ is different from the one used in previous works in two aspects: first, it represents connections between two distinct regions: the release and the collecting layer, whereas the transport matrix used for example in [5,27] quantifies the transport between boxes embedded in the same fluid region. This bipartite character of our transport matrix is shared by other operators in the literature (see, for example, [8]), but then the second difference is that in those cases transport is computed during a fixed amount of time, whereas in our case what is fixed is the distance between the two layers, with possibly different times of transport between them for different particles.

Equation (16) immediately leads to a probabilistic interpretation: $\mathbf{P}(z_0, z)_{ij} \geqslant 0$ is the probability that a particle that started at t_0 in a uniformly random position in box A_i of the release layer reaches the collecting layer for the first time on box B_j. If all the particles released from $\mathcal{M}$ reach the collecting layer, then $\mathbf{P}(z_0, z)_{ij}$ is row stochastic:

$$\sum_{j=1}^{M_z} \mathbf{P}(z_0, z)_{ij} = 1. \qquad (17)$$

If some particles never reach the collecting layer, then we can have $\sum_{j=1}^{M} \mathbf{P}(z_0, z)_{ij} < 1$, this being the probability of reaching the lower layer if starting from a random position in the release one. As when dealing with open flows [28] one can consider the transport matrix that takes into account only the particles that do reach the second layer. The so-called *out-strength* of node i, defined as

$$S_{\mathrm{OUT}}(i) = \sum_{j=1}^{M_z} \mathbf{P}_{ij}, \qquad (18)$$

can be used to formulate a general definition of the bilayer transport matrix, which is row-stochastic and valid for both closed and open flows (i.e., cases in which the collecting layer is always reached and cases in which it is not):

$$\mathbf{Q}_{ij} = \begin{cases} \frac{\mathbf{P}_{ij}}{S_{\mathrm{OUT}}(i)} & \text{if } S_{\mathrm{OUT}}(i) \neq 0 \\ 0 & \text{if } S_{\mathrm{OUT}}(i) = 0 \end{cases}. \qquad (19)$$

In the following we indicate some relevant network measures that can be computed from this bipartite transport matrix.

B. Network measures

Many quantities have been introduced to characterize the topology and connectivity properties of networks [29]. In this paper we will not consider nonlocal quantifiers, such as optimal paths, betweenness, or communities [4,5,30–32]. We just introduce the simplest quantifiers involving single nodes, namely, degrees and network entropy. The adjacency matrix is given by

$$A_{ij} = \begin{cases} 1 & \text{if } \mathbf{Q}_{ij} > 0 \\ 0 & \text{if } \mathbf{Q}_{ij} = 0 \end{cases}. \qquad (20)$$

It is used to define the out-degree of a node i, $K_{\mathrm{OUT}}(i)$, i.e., the number of nodes in layer z receiving fluid from node i in layer z_0, and the in-degree for a node j, $K_{\mathrm{IN}}(j)$, which is the number of nodes of the release layer from which fluid content arrives at node j in the collecting layer:

$$K_{\mathrm{OUT}}(i) = \sum_{j=1}^{M_z} A_{ij}, \qquad (21)$$

$$K_{\mathrm{IN}}(j) = \sum_{i=1}^{M_0} A_{ij}. \qquad (22)$$

Quantities related to degrees but that take into account the actual proportion of particles arriving at each node (the *weights* of the links) are the out-strength defined in Eq. (18) and the *in-strength*:

$$S_{\mathrm{IN}}(j) = \sum_{i=1}^{M_0} \mathbf{P}_{ij}. \qquad (23)$$

An alternative to S_{IN} can also be defined by using $\mathbf{Q}_{ij}$ instead of $\mathbf{P}_{ij}$. It coincides with (23) for closed flows, which is the case for the example presented later in this paper.

Another quantity that takes into account the weights of the links is the network entropy, defined for each node i of the release layer as

$$H(i) = -\sum_{j=1}^{M_z} \mathbf{Q}_{ij} \log(\mathbf{Q}_{ij}). \qquad (24)$$

Note that, different from previous references [5], we have not introduced a prefactor corresponding to the inverse of the integration time in the definition (24).

V. RELATIONSHIP BETWEEN GEOMETRIC AND NETWORK CHARACTERIZATION

For clarity, in the following we write expressions in terms of the matrix $\mathbf{P}_{ij}$, with the understanding that $\mathbf{Q}_{ij}$ should be used instead if the flow is open. We first obtain a relationship between the probabilistic or network approach and the geometric or dynamical one for the evolution of densities. Recall that $\mathbf{P}_{ij}$ is estimated as $\mathbf{P}_{ij} = N_{ij}/N_0$, where N_{ij} is the number of particles released from box A_i and landing

on box B_j, provided N_0 particles are seeded from each release box (giving the same density σ_0 at each initial box if all of them have the same area). Then $S_{\text{IN}}(j)$, defined in (23), is estimated as $S_{\text{IN}}(j) = N_j/N_0$, where N_j is the number of particles landing on box B_j irrespective of their origin. On the other hand, the average of the ratios of local densities $\sigma(\mathbf{x})/\sigma_0$ of the points inside a collecting box B_j, $\langle \sigma(\mathbf{x}) \rangle_{B_j}/\sigma_0 = \mu(B_j)^{-1} \int_{B_j} d\mathbf{x} \sigma(\mathbf{x})/\sigma_0$, is also estimated by N_j/N_0. These estimates become exact in the limit $N_0 \to \infty$. Using relationships (9) and (10) we find

$$S_{\text{IN}}(j) = \lim_{N_0 \to \infty} \frac{N_j}{N_0} = \langle F \rangle_{B_j} = \langle (\bar{\Lambda}_1 \bar{\Lambda}_2)^{-1} \rangle_{B_j}, \qquad (25)$$

where the left-hand side is computed from the network approach of Sec. IV, and the right-hand average is a coarse graining of quantities from the geometrically based approach of Sec. III. Note that Eq. (10) assumes the absence of folding processes producing multiple branches of arrival of the release layer onto the collecting one, so that this is also needed for the validity of (25).

We now suggest some network-geometric relationships similar to the ones developed in [5] for single-layer Lagrangian flow networks. In particular, relationships between degree and network entropy on the one hand and the largest stretching factor and Lyapunov exponent on the other were found. These relationships were not exact ones, but approximate relationships that were checked to hold for the case of long times, sufficiently small network boxes, and a clear hyperbolic situation (i.e., Lyapunov exponents sufficiently larger or smaller than zero).

By repeating the heuristic arguments developed in [5] we can find the following approximate relationships between the network and the geometrical description of our two-layer dynamics:

$$K_{\text{OUT}}(i) \approx \langle \bar{\Lambda} \rangle_{A_i} = \langle e^{|z-z_0|\bar{\lambda}} \rangle_{A_i}, \qquad (26)$$

$$H(i) \approx \langle \log \bar{\Lambda} \rangle_{A_i} = |z - z_0| \langle \bar{\lambda} \rangle_{A_i}, \qquad (27)$$

where $\bar{\Lambda}$ and $\bar{\lambda}$ are defined below. The averages perform a coarse graining of the values of $\bar{\Lambda}(\mathbf{x}_0)$ or $\bar{\lambda}(\mathbf{x}_0)$ over all initial conditions inside the initial box A_i. Different from the bidimensional situation considered in [5], in which only one of the stretching factors was larger than one (a single expanding direction), in the present three-dimensional dynamics several directions can be expanding, and these directions are, in the arguments leading to Eqs. (26) and (27), the ones that contribute to the out-degree K_{OUT} or to the network entropy H. In consequence, in Eqs. (26) and (27) we should use for every initial location $\bar{\Lambda} \equiv \prod_\alpha \bar{\Lambda}_\alpha$, where the product is over all factors $\bar{\Lambda}_\alpha$ that satisfy $\bar{\Lambda}_\alpha > 1$ at that point, or, equivalently, $\bar{\lambda} \equiv \sum_\alpha \bar{\lambda}_\alpha$, where the sum is over all positive FDLEs, $\bar{\lambda}_\alpha > 0$, at that point.

We stress that relationships (26) and (27) are not exact, but we expect them to be satisfied for sufficiently small network boxes, large $|z - z_0|$, and dynamics sufficiently hyperbolic, which roughly requires $\bar{\Lambda}_\alpha$ sufficiently different from unity. We will check this validity for a particular flow model in Sec. VI E.

VI. NUMERICAL RESULTS

In this section we illustrate the previous concepts with a slightly modified version of an idealized incompressible 3D flow, the ABC flow.

A. ABC flow model

The ABC flow is a 3D model flow which is widely used for analyzing chaotic transport [33,34]. It provides a simple stationary solution of Euler's equation for incompressible, inviscid fluid flows.

To simulate the situation of particles going from one layer to another, we modify the ABC flow with a drift in a preferential direction, specifically in the vertical one (z-direction), without changing most of the properties of the flow. The motivation for this choice is to mimic in a very simple way the transport of particles falling under gravity in a chaotic fluid flow. The equations describing the model are

$$\dot{x} = v_x = A \sin z + C \cos y, \qquad (28)$$

$$\dot{y} = v_y = B \sin x + A \cos z, \qquad (29)$$

$$\dot{z} = v_z = C \sin y + B \cos x + D. \qquad (30)$$

We take $A = 1, B = \sqrt{2}, C = \sqrt{3}$ for which chaotic motion is found [34]. The constant $D = -3.15$ is the one giving a contribution to the velocity pointing downwards. Its value is just sufficient to keep the particles traveling downwards in the z direction (thus, $v_z < 0$ for any particle at any time). Among other consequences, this guarantees that all initially released trajectories will reach the collecting layer at some time, so that $S_{\text{OUT}} = 1$ in Eq. (18). In the horizontal coordinates the fluid domain is $x, y \in [0, 2\pi]$ with periodic boundary conditions. In the vertical (z-coordinate) particles are released from the layer $z_0 = 10$ and are followed until they reach the layer at coordinate z where integration is stopped. Thus the model is defined in the vertical interval $[z, z_0]$.

Note that $\nabla \cdot \mathbf{v} = 0$. The facts that $v_z < 0$ and that the flow is time-independent guarantee that the map $\phi_{z_0}^z$ is one-to-one.

B. Transport properties between layers

We first study the map $\phi_{z_0}^z$ for the ABC flow by taking $z_0 = 10$ and $z = 0$ (particles fall from height z_0). In Fig. 3 we show a histogram of arrival times, $p(\omega)$. It shows a two-peaked shape with peaks around the values 2 and 6. We can differentiate two main dynamical behaviors: more laminar for the first peak and more chaotic for the second one. This suggests the existence of two zones of trajectory behavior in the fluid flow, which is confirmed in Fig. 4.

We show in Fig. 4 the spatial distribution of ω, the time needed by every particle to go from layer z_0 to layer z. This time is shown as a color map for every particle at the release layer z_0 and on its corresponding final position at layer z. The color map in the bottom layer is conveniently computed by running the flow backwards in time from a regular grid of initial conditions located at z. The equivalence between the backwards- and the forward-in-time calculation of ω is guaranteed by the fact that for this time-independent flow the map $\phi_{z_0}^z$ is one-to-one. Since $v_z < 0$ for any particle and time,
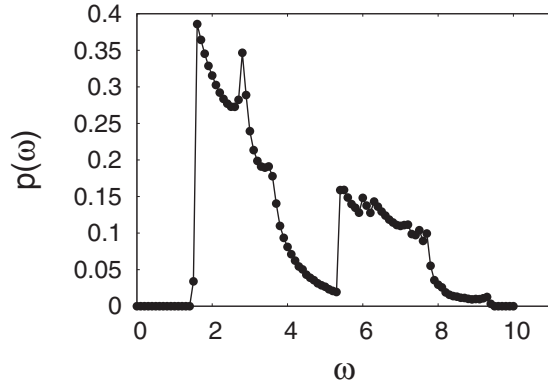
FIG. 3. Histogram of the times to reach the second layer at $z = 0$, starting from $z_0 = 10$.

all particles released in the upper layer reach the collecting layer in a finite time, and all locations in the collecting layer receive a trajectory.

We observe the two mentioned regions in Fig. 4: the first peak in Fig. 3 corresponds to the dark regions, with more laminar trajectories, i.e., the particles go straightforwardly from one layer to the other; and the red regions correspond to the second peak and to more convoluted (chaotic) trajectories. The frontiers between initial conditions of large and small ω are quite sharp and will be identified with lines of large finite-depth Lyapunov exponent in Sec. VI C.

C. Geometric characterization

The Jacobian $\bar{\boldsymbol{J}}_{\mathcal{M}}$ is computed by releasing particles on a regular grid on layer z_0, integrating their trajectories under the modified ABC flow until reaching the final layer at z, and approximating the derivatives in $\bar{\boldsymbol{J}}_{\mathcal{M}} = \boldsymbol{\nabla}\phi_{z_0}^z(\mathbf{x}_0)$ by finite differences between final positions of initially neighboring particles. Then its singular values $\bar{\Lambda}_1$ and $\bar{\Lambda}_2$ are computed after construction of the Cauchy-Green tensor $\bar{C}_{\mathcal{M}} = \bar{\boldsymbol{J}}_{\mathcal{M}}^T \bar{\boldsymbol{J}}_{\mathcal{M}}$.

Figure 5 shows the maximal FDLE $\bar{\lambda}_1(\mathbf{x}_0)$ from Eq. (7), displayed on the release layer $z_0 = 10$, for collecting layers at three different depths z. We see that increasingly finer filamentary structures appear for increasing travel depth. This is similar to the behavior of the FTLE for increasing integration time. We note that the highest FDLE values
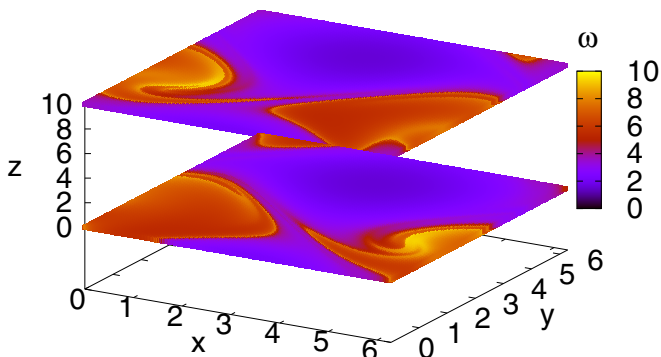

FIG. 4. The travel time, ω, from release layer ($z_0 = 10$) to collecting layer ($z = 0$) displayed at the initial and final position of each particle.
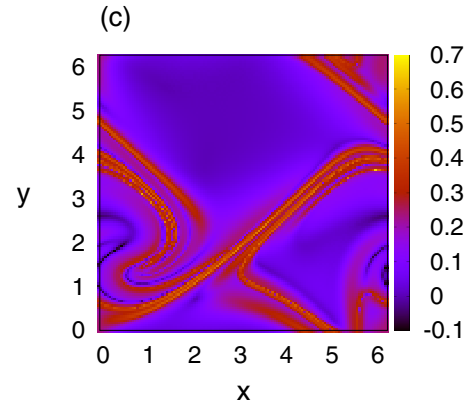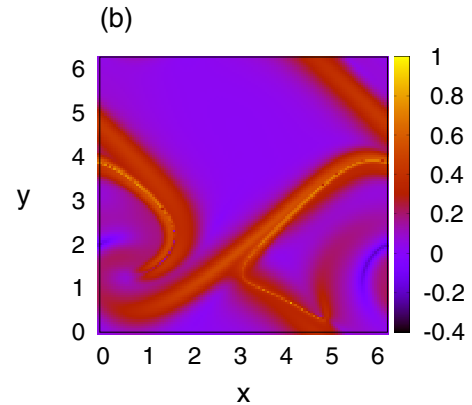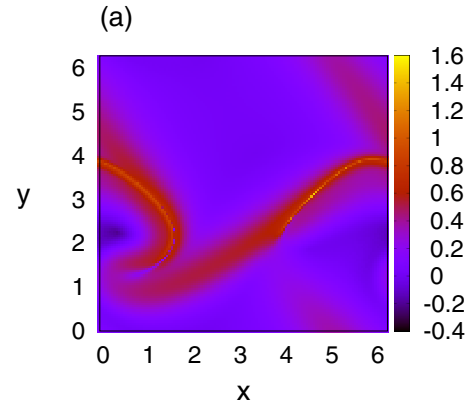

FIG. 5. Maximal FDLE $\bar{\lambda}_1$ for dynamics under the modified ABC flow, displayed at the initial particle locations in the release layer $z_0 = 10$, and for the collecting layer at (a) $z = 2\pi$, (b) $z = 4$, and (c) $z = 0$.

roughly divide the release domain into two regions (remember the periodic boundary conditions in the horizontal directions) that closely correspond to the long and short travel time regions in Fig. 4: as for the FTLE, ridges of the FDLE are associated with separatrices that divide the release layer into regions of different dynamic behavior. In particular, these structures are reminiscent of a stable foliation corresponding to hyperbolic trajectories. Although periodic trajectories cannot exist when $v_z < 0$ everywhere in a domain with a finite vertical extension at any time, they can exist in the same velocity field with periodic boundary conditions in the vertical direction. Finite portions of such trajectories will
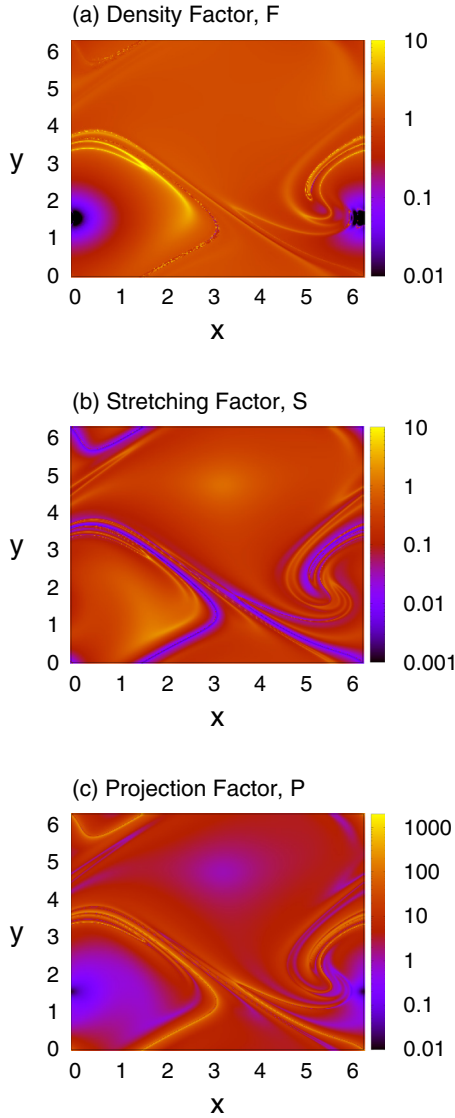
FIG. 6. (a) The density factor, F, computed as $F = (\bar{\Lambda}_1 \bar{\Lambda}_2)^{-1}$ at the collecting layer $z = 0$, giving the relative density of collected particles if the density in the release layer $z_0 = 10$ is uniform. (b) The stretching factor S, computed as $S = (\Lambda_1 \Lambda_2)^{-1}$. (c) The projection factor P from Eq. (13). We have checked that $F = SP$ to good accuracy. Note the logarithmic scale in the color maps.

govern finite-time chaotic dynamics through finite-length versions of the corresponding stable and unstable manifolds that appear according to the extent of the domain in the z direction when periodicity is not prescribed for that coordinate. Ridges in the FTLE field would arise from intersections with the release layer of these finite-length stable manifolds, and this also happens at the same locations in the FDLE field, as seen in Fig. 5, in spite of the complication that arises from the projection effect included in the definition of the FDLE. In fact, we have checked (not shown) that these intersections are much more clearly identified in the FDLEs than in the FTLEs.

It also appears that there is a correspondence between the intersections with the collecting layer of finite-length unstable manifolds and ridges in the density factor F: in Fig. 6(a) we plot the factor F on the collecting layer, which is the factor
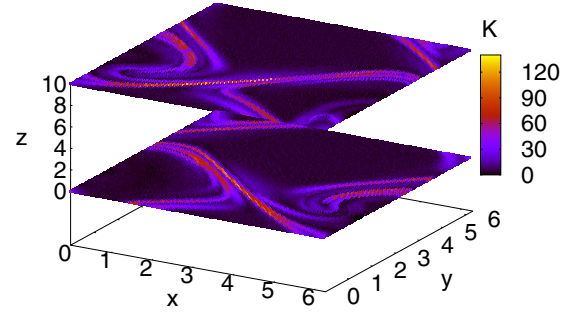

FIG. 7. Out-degree and in-degree in the release ($z_0 = 10$) and the collecting ($z = 0$) layers, respectively.

that multiplies the initial density at the release layer (and thus it is proportional to the accumulated density of particles if the release density is constant). We also display in the other panels of Fig. 6 the two geometric factors, stretching S and projection P, that shape F [i.e., $F = SP$, Eq. (11)]. We see clearly from the plot of F that filamentary structures will appear in the density collected in the lower layer. The effect of surface-element stretching (S) is less determinant for F than the projection of surface elements onto the collecting layer (P), although this can be different for other types of flows. In more complex flows [20–22] the projection factor can even diverge at *caustics*, locations where the denominator of Eq. (13) vanishes. As in [20], there is some degree of anticorrelation between S and P, so that the fluctuations in F are smaller than those in S and P.

D. Network characterization

We study connectivity properties between layers $z_0 = 10$ and $z = 0$. For doing this, we divide the upper layer into 100×100 square boxes A_i, $i = 1, \ldots, 10\,000$, and the lower one into 100×100 square boxes B_j, $j = 1, \ldots, 10\,000$. Then we release from each box in z_0 900 particles uniformly distributed. We integrate each of these particles with the map $\phi_{z_0}^z$ [equivalent to integrating Eq. (1) until reaching the collecting layer at z].

In Fig. 7 we show the out-degree in the starting layer and the in-degree in the final one. The out-degree for a given box in the starting layer indicates the number of boxes reached in the final layer. It is a measure of dispersion, and large values at a box indicate that a part of a repelling or dispersing structure is present there. On the other hand, large in-degree values in the final layer indicate mixing from a large number of different initial boxes, so that boxes with in-degree maxima trace out the location of attracting regions. Part of these ideas is confirmed when comparing out-degrees to the FDLEs of Fig. 5(c).

Another quantity computed in the network approach, the entropy $H(i)$ defined in Eq. (24), is displayed in Fig. 8. There is a clear relationship with $K_{\rm OUT}(i)$ (Fig. 7) and also with the FDLEs of Fig. 5(c). These relationships will be checked more systematically in the next section.

E. Relationship between geometric and network characterization

In this section we first check Eq. (25). It relates the network quantity $S_{\rm IN}(j)$, giving also the density accumulated at box B_j
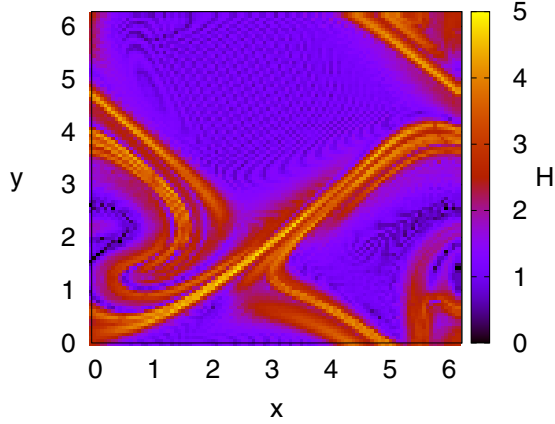
FIG. 8. Entropy $H(i)$ for transport from the release layer at $z_0 = 10$ to the collecting layer at $z = 0$, displayed on the release layer.

in the lower layer relative to the uniform release density in the upper layer, to a coarse graining on collecting boxes of a quantity developed in the geometric approach, the density factor $F = (\bar{\Lambda}_1 \bar{\Lambda}_2)^{-1}$. In Fig. 9 we see that, as predicted, both quantities are nearly equal, although there are some
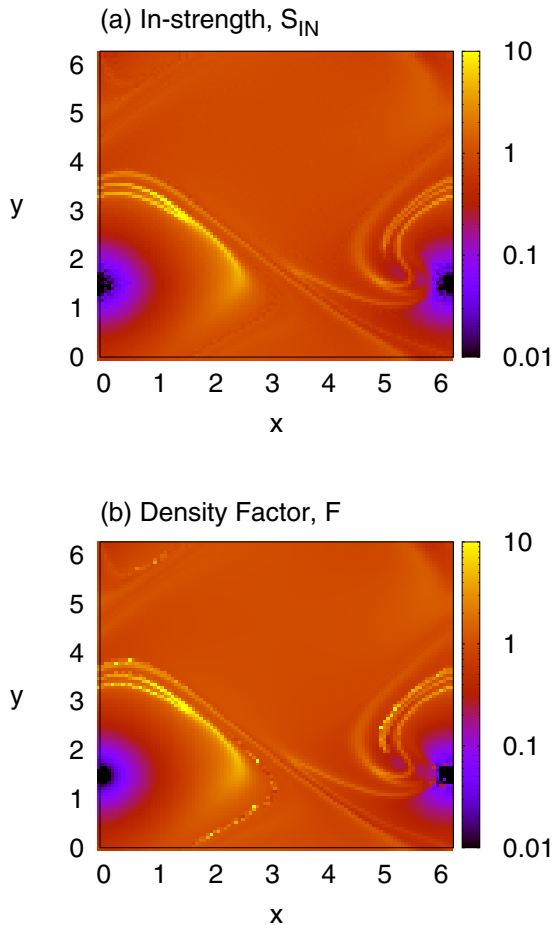

FIG. 9. (a) The in-strength $S_{\mathrm{IN}}(j)$ in the lower layer $z = 0$, which gives the accumulated density in that layer starting from a unit-density uniform release at $z_0 = 10$. (b) Density factor averaged on each box of the accumulation layer, i.e., $\langle F \rangle_{B_j} = \langle (\bar{\Lambda}_1 \bar{\Lambda}_2)^{-1} \rangle_{B_j}$.
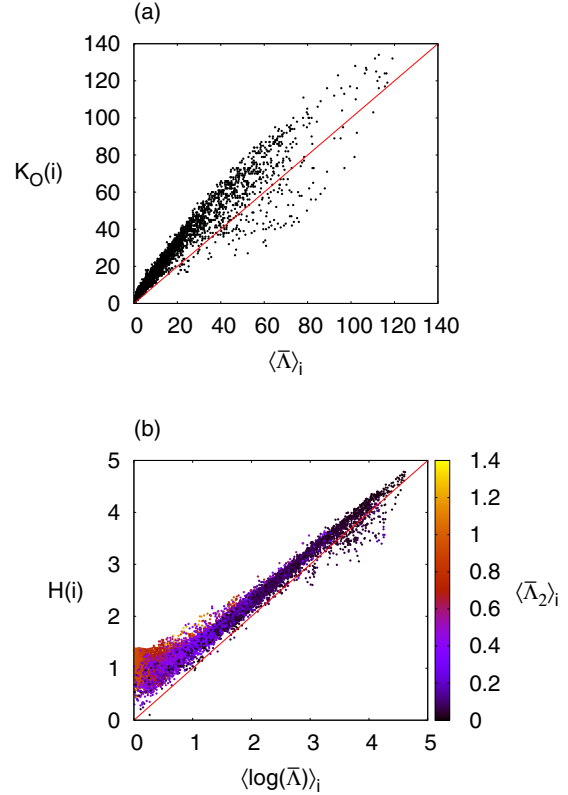

FIG. 10. (a) Scatter plot of values of $K_{\mathrm{OUT}}(i)$ vs $\langle \bar{\Lambda} \rangle_{A_i}$. The red diagonal indicates the fulfillment of Eq. (26). (b) Scatter plot of values of $H(i)$ vs $\langle \log \bar{\Lambda} \rangle_{A_i}$. The red diagonal indicates the fulfillment of Eq. (27). Dots are colored according to the value of $\langle \bar{\Lambda}_2 \rangle_{A_i}$.

differences in the narrowest filamental regions, arising from numerical inaccuracies. According to the outlying values in Fig. 9(b), it is presumably S_{IN} that can be computed more reliably than $(\bar{\Lambda}_1 \bar{\Lambda}_2)^{-1}$.

We now address the validity of expressions (26) and (27). Differently from Eq. (25), these formulas were derived only heuristically, following the arguments of Ref. [5]. Their validity is subjected to restrictions such as smallness of boxes, large values of $|z - z_0|$, and sufficiently hyperbolic dynamics (roughly, singular values sufficiently different from unity), which we will now check if are satisfied for our modified ABC flow.

Regarding Eq. (26), comparison of K_{OUT} from the upper layer in Fig. 7 and $\bar{\lambda}_1$ in Fig. 5(c), which is the logarithm of $\bar{\Lambda}_1$, already indicates a strong relationship. A more quantitative comparison is made in Fig. 10(a) between $K_{\mathrm{OUT}}(i)$ and $\langle \bar{\Lambda} \rangle_{A_i}$, where $\Lambda = \prod_\alpha \bar{\Lambda}_\alpha$ is the product of all singular values larger than unity. We see that, although there is a positive correlation, there is no identity between the two quantities. We attribute this failure of Eq. (26) to the fact that the second singular value $\bar{\Lambda}_2$ takes values smaller but close to unity for most of the trajectories. This is confirmed by the distribution of $\bar{\Lambda}_2$ in the upper layer displayed in Fig. 11. We note that, since the modified ABC flow is time independent, we always have that the second Lyapunov exponent is zero, or $S_2 = 1$. The three-dimensional singular value S_2 is not exactly Λ_2 nor $\bar{\Lambda}_2$, but it is related to them at long times, which justifies the
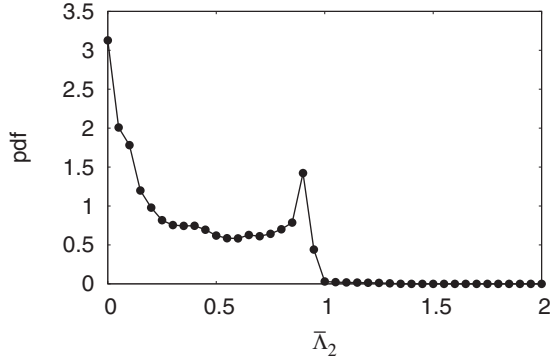
FIG. 11. Probability density function of the values of $\bar{\Lambda}_2$ on the release layer.

prevalence of values $\bar{\Lambda}_2 \approx 1$ in Fig. 11, and then a lack of hyperbolicity. $\bar{\Lambda}_2 \approx 1$ implies that boxes in the upper layer are not converted by the dynamics into thin filaments, as when $\bar{\Lambda}_2 \ll 1$, but into broad strips. When reaching the collecting layer, they will leave a footprint larger than the thin filament implied in Eq. (26) when $\bar{\Lambda}_2 < 1$, and consequently K_{OUT} will be generally larger than predicted, as seen in Fig. 10(a).

Relationships that imply a weighting with the number of particles reaching a particular box in the collecting layer are expected to be more robust than relations such as Eq. (26) that involve the degree, a quantity counting all boxes to which particles arrive, independently on how many of them do so. Thus, Eq. (27), although derived under heuristic arguments similar to those leading to Eq. (26), is expected to be satisfied under a broader range of conditions. This is indeed the case, as seen by comparing plots of entropy (Fig. 8) with corresponding plots of FDLE [Fig. 5(c)]. A more quantitative check is performed in Fig. 10(b). We see that the equality in Eq. (27) is satisfied much better than Eq. (26). Nevertheless, there are still deviations, especially for small values of $\langle \log \bar{\Lambda} \rangle_{A_i}$. These small values arise from locations where $\bar{\Lambda} \approx 1$, confirming situations of lack of hyperbolicity. We have also colored the points in the scatter plot with the values of $\langle \bar{\Lambda}_2 \rangle_{A_i}$. Again, the stronger deviations occur when both $\langle \bar{\Lambda}_2 \rangle_{A_i}$ and $\langle \bar{\Lambda} \rangle$ are close to unity.

VII. CONCLUSIONS

In this paper we have developed a formalism to characterize transport of particles between two layers in a fluid. The motivation was to obtain a theoretical framework to analyze problems related to the sinking of particles in fluid flows, sedimenting towards a bottom layer. Two complementary sets of tools have been addressed: geometrical or dynamical, by studying the dynamics and deformation of a layer of particles, and probabilistic, using concepts from network theory. Most importantly, we have addressed the relationship between these two approaches, and illustrated the whole formalism with a modified ABC model.

The crucial step is the definition of a two-layer map, which drives particles from an initial layer to the final one. Within the geometric approach we have analyzed the deformation of surfaces and lines of particles released from the upper

layer. A quantity related to the Lyapunov exponent, the FDLE, has been defined and related to the quantities above. Within the probabilistic methodology the natural description of the system is via bipartite networks, in which quantities such as the out-degree in the initial layer and the in-degree in the final one acquire a clear physical meaning. Both descriptions have been connected, for example, by expressing the accumulated density of particles in terms of the in-degree and of averages of singular values defined in the geometric approach. Other geometric-network relationships that were successfully tested for transport on a single layer [5] are satisfied here with poor accuracy. This stresses the need for sufficiently hyperbolic dynamics to justify some of the heuristic steps used in the derivations.

More explicitly, the two-layer map provides a general description of particle transport between layers, without any restriction to hyperbolic flows or transport without folding. This means that most of the geometric and network formalism described in Secs. III and IV, respectively, can be applied to any type of flow. However, some of the specific relationships we have obtained, namely, Eqs. (10) and (25)–(27), require the validity of additional hypotheses that we now detail.

The heuristic arguments leading to Eqs. (26) and (27), which link the geometrical perspective with the network-based description, are restricted to sufficiently hyperbolic dynamics, meaning in this context that $\bar{\Lambda}_1$ and $\bar{\Lambda}_2$ should be sufficiently different from unity. Thus, these two relationships will be valid only in regions dominated by strain. Unlike in two-dimensional incompressible flows where it is sufficient to take care of one singular value of the Jacobian matrix [20], the second singular value of $\bar{J}_M$ in three-dimensional flows is independent of the first one and thus also plays a role. If this second singular value $\bar{\Lambda}_2$ is close to unity, fluid patches released from the upper layer may be converted into broad strips after being projected onto the collecting layer, which results in a deviation from Eqs. (26) and (27). This dependence on the second singular value is illustrated in Fig. 10(b).

On the other hand, folding of the falling surface, which may occur in time-dependent flows, affects our formalism in two ways. The first is that the inverse of the two-layer map, appearing in (16), is multivalued if foldings are present, for which Eqs. (10) and (25) have to be modified (as done in [20,22]) to take into account all preimages of each given point in the collecting layer. The second is that the singular values of the Jacobian matrix $\bar{J}_M$ are ill-defined at folds, so that the evaluation of FDLEs and the density factor F becomes impossible there as well. The decomposition $F = SP$ and the divergence of P shows, in fact, that F also diverges at folds, identifying the appearance of caustics (cf. [20]).

Note that we have assumed homogeneity in the initial distribution of particles to focus on the effects of transport. If one is interested in analyzing the evolution of nonhomogeneous initial particle distributions, the density at the collecting layer can be simply recovered by multiplying the initial density by the corresponding density factor of each particle trajectory reaching the bottom layer. Thus, final densities can always be computed if the initial density of particles at the release layer is known.

There are recent works studying, on the one hand, microplankton sedimentation in the ocean with network tools

[35] and, on the other, the geometry of sedimentation dynamics and distribution of biogenic particles [12,21] and microplastics [17]. We have presented here steps that connect both approaches, and that may provide insights into problems of sinking particles in the ocean. In particular, the FDLE is a measure specifically defined for the study of flow patterns between two layers with a preferential direction of motion and quantifies structures in a different way if compared to standard geometrical measures, such as the classical finite-time Lyapunov exponent. For example, FDLE ridges neatly separate regions in upper and lower layers in which particle travel times are significantly different (compare Figs. 4 and 5). Also, while the decomposition of F into S and P is not new in itself, we have provided here alternative ways to compute F and S. Such a decomposition is crucial for exploring and quantifying the relative contributions of the stretching factor S and the projection factor P to the resulting distribution of particles when being collected after a sedimentation process. In general terms, our formalism characterizes repelling and attracting structures associated with transport between both layers. The result is a theoretical characterization that may be useful in future applications that focus on transport properties of sinking particles, such as the study of sedimentation patterns, and barriers between regions with qualitatively different dynamics. Furthermore, community detection approaches that become accessible due to the network characterization can be practically useful, as has been the case in situations of horizontal transport [5].

Comparing the approach of Sec. IV to that in [35] where bilayer networks are also used, the crucial differences are that [35], using a backwards-in-time approach, focuses on the origin over the surface of the particles deposited on the sea floor, and that those authors are interested in a statistical description over paleoscales. In contrast, our network approach is based on a forward-in-time integration, so that we focus on the fate of the particles after being released from the surface. We thus identify flow structures at the timescales during which the particles move from one layer to another, and we relate them to the geometry of a falling layer. All of this is suited to the application to mesoscale and submesoscale transport in the marine environment, at timescales from days to months. This will be also relevant for studies of sedimentation in atmospheric flows, such as in the context of deposition of volcanic ashes or aerosol particles [36,37]. More generally, we expect our formalism to be of use in other flow problems in which a dominant direction of transport occurs.

APPENDIX

In this Appendix we give further details on the geometry of projection and stretching that is used in the geometric approach.
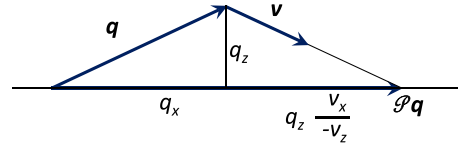

FIG. 12. Sketch (in a two-dimensional situation) of the footprint or projection in the direction of motion, $\mathcal{P}\mathbf{q}$, of a vector $\mathbf{q} = (q_x, q_y)$ onto a horizontal collecting layer (in fact a collecting line) when arriving there with velocity $\mathbf{v} = (v_x, v_y)$. We have $\mathcal{P}\mathbf{q} = (q_x - q_z v_x/v_z)\hat{\mathbf{x}}$, where $\hat{\mathbf{x}}$ is the unit vector in the direction of the collecting line.

proach. Some of the expressions presented here were already derived or used in Refs. [20–22].

First, we derive expressions for the footprint left by a vector $\mathbf{q}$ on the collecting layer as it arrives in it with a velocity $\mathbf{v}$. We will apply the expressions to vectors tangent to the falling surface that represent infinitesimal segments of that surface. Thus the velocity vector $\mathbf{v}$ is evaluated at the center point of the falling segment when it touches the collecting layer at t_z and, because of the segment's infinitesimal character, the same $\mathbf{v}$ applies to the whole vector $\mathbf{q}$. Figure 12 shows a sketch of the geometry in a two-dimensional situation, so that the components of the vector are (q_x, q_z) and those of the velocity (v_x, v_z). The horizontal projection $\mathcal{P}\mathbf{q}$ of $\mathbf{q}$ along the direction of motion, or footprint, is made of two parts: q_x and the result of multiplying q_z by the tangent of the angle between $\mathbf{v}$ and the vertical, i.e., $q_z v_x/(-v_z)$. Considering also the y component, the projected vector is $\mathcal{P}\mathbf{q} = (q_x - q_z v_x/v_z, q_y - q_z v_y/v_z)$ and the vertical component $(\mathcal{P}q)_z$ is zero. The projection of $\mathbf{q} = (q_x, q_y, q_z)$ onto the direction of motion is a linear operation, and thus it can be expressed as the action of a matrix $\mathcal{P}$ on the vector, with

$$\mathcal{P} = \begin{pmatrix} 1 & 0 & -v_x/v_z \\ 0 & 1 & -v_y/v_z \end{pmatrix}. \tag{A1}$$

A row of zeros can be added to the bottom if $\mathcal{P}\mathbf{q}$ is considered to be embedded in three-dimensional space. An equivalent expression for this projection operator can be written in terms of cross products:

$$\mathcal{P}\mathbf{q} = \hat{\mathbf{z}} \times \left(\mathbf{q} \times \frac{\mathbf{v}}{v_z} \right), \tag{A2}$$

where $\hat{\mathbf{z}}$ is the unit vector in the positive vertical direction.

Let us consider a vector of the form $\boldsymbol{\tau}(t) = \frac{d\phi_{t_0}^\tau[\mathbf{x}_0(s)]}{ds}$, which is tangent to the falling surface at every time, and points initially (at time t_0) along the direction on the release layer specified by the parameter s. $\bar{\boldsymbol{\tau}} = \bar{\boldsymbol{J}}_{\mathcal{M}} \cdot \boldsymbol{\tau}(t_0)$ is its footprint on the collection layer. The generation of this footprint (see Fig. 1) results from the composition of two transformations, namely, the three-dimensional stretching as the falling surface is advected towards the collecting surface, $\boldsymbol{\tau}(t_z) = \boldsymbol{J}_{\mathcal{M}} \cdot \boldsymbol{\tau}(t_0)$, and its subsequent projection onto the horizontal along the direction of motion, $\bar{\boldsymbol{\tau}} = \mathcal{P}\boldsymbol{\tau}(t_z)$. The combination of these two processes gives the following relationship:

$$\bar{\boldsymbol{J}}_{\mathcal{M}} = \mathcal{P}\boldsymbol{J}_{\mathcal{M}}. \tag{A3}$$

This expression can be derived more formally by applying the chain rule to Eq. (4), as done explicitly in [20] for the two-dimensional case. Since the singular values of $\mathcal{P}$ are $|\mathbf{v}|/|v_z|$ and 1, standard inequalities for singular values of products of matrices [26] allow us to show that $\bar{\Lambda}_1 \leqslant \Lambda_1 |\mathbf{v}|/|v_z|$ and $\bar{\Lambda}_1 \bar{\Lambda}_2 \leqslant |\mathbf{v}/v_z| \Lambda_1 \Lambda_2$. This last inequality is improved, however, by the exact equality in Eq. (15).

We now obtain expression (13) for the projection factor P entering the density factor. We first note that $\bar{\boldsymbol{\tau}}_x = \mathcal{P} \boldsymbol{\tau}_x(t_z)$ and $\bar{\boldsymbol{\tau}}_y = \mathcal{P} \boldsymbol{\tau}_y(t_z)$. Thus, we can elaborate the expression for the density factor in Eq. (9) (we omit the time variable t_z to simplify the notation):

$$F^{-1} = |\bar{\boldsymbol{\tau}}_x \times \bar{\boldsymbol{\tau}}_y| = |\mathcal{P} \boldsymbol{\tau}_x \times \mathcal{P} \boldsymbol{\tau}_y|$$
$$= \left| \left[\hat{\boldsymbol{z}} \times \left(\boldsymbol{\tau}_x \times \frac{\mathbf{v}}{v_z} \right) \right] \times \left[\hat{\boldsymbol{z}} \times \left(\boldsymbol{\tau}_y \times \frac{\mathbf{v}}{v_z} \right) \right] \right|$$

$$= \frac{1}{v_z^2} |[\boldsymbol{\tau}_x (\hat{\boldsymbol{z}} \cdot \mathbf{v}) - \mathbf{v}(\hat{\boldsymbol{z}} \cdot \boldsymbol{\tau}_x)] \times [\boldsymbol{\tau}_y (\hat{\boldsymbol{z}} \cdot \mathbf{v}) - \mathbf{v}(\hat{\boldsymbol{z}} \cdot \boldsymbol{\tau}_y)]|$$

$$= \frac{1}{v_z^2} |[\boldsymbol{\tau}_x v_z - \mathbf{v}(\tau_x)_z] \times [\boldsymbol{\tau}_y v_z - \mathbf{v}(\tau_y)_z]|$$

$$= \frac{1}{|v_z|} |v_z(\boldsymbol{\tau}_x \times \boldsymbol{\tau}_y) + (\tau_x)_z(\boldsymbol{\tau}_y \times \mathbf{v}) - (\tau_y)_z(\boldsymbol{\tau}_x \times \mathbf{v})|$$

$$= \left| \frac{(\boldsymbol{\tau}_x \times \boldsymbol{\tau}_y) \cdot \mathbf{v}}{v_z} \hat{\boldsymbol{z}} \right|$$

$$= \left| \frac{\hat{\mathbf{n}} \cdot \mathbf{v}}{v_z} \right| |\boldsymbol{\tau}_x \times \boldsymbol{\tau}_y|. \tag{A4}$$

Comparing with Eqs. (11) and (12) we identify the projection factor $P = |v_z/(\hat{\mathbf{n}} \cdot \mathbf{v})|$, thus demonstrating Eq. (13).

[1] J. M. Ottino, *The Kinematics of Mixing: Stretching, Chaos, and Transport* (Cambridge University Press, Cambridge, 1989).

[2] S. Wiggins, Annu. Rev. Fluid Mech. **37**, 295 (2005).

[3] S. C. Shadden, F. Lekien, and J. E. Marsden, Physica D **212**, 271 (2005).

[4] E. M. Bollt and N. Santitissadeekorn, *Applied and Computational Measurable Dynamics* (SIAM, New York, 2013).

[5] E. Ser-Giacomi, V. Rossi, C. López, and E. Hernández-García, Chaos **25**, 036404 (2015).

[6] G. Froyland, R. M. Stuart, and E. van Sebille, Chaos **24**, 033126 (2014).

[7] G. Froyland, K. Padberg, M. H. England, and A. M. Treguier, Phys. Rev. Lett. **98**, 224503 (2007).

[8] G. Froyland, C. Horenkamp, V. Rossi, and E. van Sebille, Chaos **25**, 083119 (2015).

[9] J. H. Bettencourt, C. López, E. Hernández-García, I. Montes, J. Sudre, B. Dewitte, A. Paulmier, and V. Garçon, Nat. Geosci. **8**, 937 (2015).

[10] J. H. Bettencourt, V. Rossi, E. Hernández-García, M. Marta-Almeida, and C. López, J. Geophys. Res. Oceans **122**, 7433 (2017).

[11] D. A. Siegel and W. G. Deuser, Deep-Sea Res. I **44**, 1519 (1997).

[12] P. Monroy, E. Hernández-García, V. Rossi, and C. López, Nonlinear Process. Geophys. **24**, 293 (2017).

[13] C. L. Sabine, R. A. Feely, N. Gruber, R. M. Key, K. Lee, J. L. Bullister, R. Wanninkhof, C. S. Wong, D. W. R. Wallace, B. Tilbrook *et al.*, Science **305**, 367 (2004).

[14] C. L. De La Rocha and U. Passow, Deep Sea Res. II **54**, 639 (2007).

[15] C. A. Choy, B. H. Robison, T. O. Gagne, B. Erwin, E. Firl, R. U. Halden, J. A. Hamilton, K. Katija, S. E. Lisin, C. Rolsky *et al.*, Sci. Rep. **9**, 1 (2019).

[16] M. L. A. Kaandorp, H. A. Dijkstra, and E. van Sebille, Environ. Sci. Technol. **54**, 11980 (2020).

[17] R. de la Fuente, G. Drótos, E. Hernández-García, C. López, and E. van Sebille, Ocean Sci. **17**, 431 (2021).

[18] E. E. Michaelides, J. Fluids Eng. **125**, 209 (2003).

[19] G. Falkovich, A. Fouxon, and M. Stepanov, Nature (London) **419**, 151 (2002).

[20] G. Drótos, P. Monroy, E. Hernández-García, and C. López, Chaos **29**, 013115 (2019).

[21] P. Monroy, G. Drótos, E. Hernández-García, and C. López, J. Geophys. Res. Oceans **124**, 4744 (2019).

[22] A. Sozza, G. Drótos, E. Hernández-García, and C. López, Phys. Fluids **32**, 075104 (2020).

[23] E. Aurell, G. Boffetta, A. Crisanti, G. Paladin, and A. Vulpiani, J. Phys. A: Math. Gen. **30**, 1 (1997).

[24] J. H. Bettencourt, C. López, and E. Hernández-García, J. Phys. A: Math. Theor. **46**, 254022 (2013).

[25] M. Cencini and A. Vulpiani, J. Phys. A: Math. Theor. **46**, 254019 (2013).

[26] R. A. Horn and C. R. Johnson, *Topics in Matrix Analysis* (Cambridge University Press, Cambridge, 1991).

[27] G. Froyland and M. Dellnitz, SIAM J. Sci. Comput. **24**, 1839 (2003).

[28] E. Ser-Giacomi, V. Rodríguez-Méndez, C. López, and E. Hernández-García, Eur. Phys. J. Spec. Top. **226**, 2057 (2017).

[29] M. E. J. Newman, *Networks: An Introduction* (Oxford University Press, Oxford, 2010).

[30] E. Ser-Giacomi, R. Vasile, E. Hernández-García, and C. López, Phys. Rev. E **92**, 012818 (2015).

[31] E. Ser-Giacomi, R. Vasile, I. Recuerda, E. Hernández-García, and C. López, Chaos **25**, 087413 (2015).

[32] E. Ser-Giacomi, A. Baudena, V. Rossi, M. Follows, S. Clayton, R. Vasile, C. López, and E. Hernández-García, Nat. Commun. **12**, 4935 (2021).

[33] T. McMillen, J. Xin, Y. Yu, and A. Zlatoš, SIAM J. Appl. Dyn. Syst. **15**, 1753 (2016).

[34] T. Dombre, U. Frisch, J. M. Greene, M. Hénon, A. Mehr, and A. M. Soward, J. Fluid Mech. **167**, 353 (1986).

[35] P. D. Nooteboom, P. K. Bijl, E. van Sebille, A. S. von der Heydt, and H. A. Dijkstra, Paleocean. Paleoclimatol. **34**, 1178 (2019).

[36] T. Haszpra and T. Tél, J. Phys.: Conf. Ser. **333**, 012008 (2011).

[37] T. Haszpra, Chaos **29**, 071103 (2019).